Demonstration of the auxiliary-field Monte Carlo approach for *sd*-shell nuclei

W. E. Ormand, D. J. Dean, C. W. Johnson,* G. H. Lang, and S. E. Koonin
W. K. Kellogg Radiation Laboratory, 106-38, California Institute of Technology, Pasadena, California 91125
(Received 14 July 1993)

We apply the auxiliary-field Monte Carlo approach to the nuclear shell model in the $1s$-$0d$ configuration space. The Hamiltonian was chosen to have isovector pairing and isoscalar multipole-multipole interactions, and the calculations were performed within the fixed-particle, canonical ensemble. The results demonstrate the feasibility of the method for $N \neq Z$ even-even and odd-odd $N = Z$ nuclei. In particular, static observables for even-even Ne isotopes and ^{22}Na compare well with results obtained from exact diagonalization of the Hamiltonian. Response functions are presented for ^{22}Ne and compared with exact results, and the viability of cranked calculations for $N \neq Z$ even-even nuclei is addressed. We present methods for computing observables in the canonical ensemble using Fourier extraction, and for determining the nuclear shape.

PACS number(s): 21.60.Cs, 21.60.Ka, 02.70.−c

I. INTRODUCTION

The shell model is one of the most successful descriptions of many-fermion systems [1]. In this picture, valence particles are spatially confined by a one-body potential and influence each other via a residual two-body interaction. Mathematically, the shell model can be reduced to a matrix-diagonalization problem by computing the matrix elements of the Hamiltonian between a set of basis states that span the configuration space of interest. There are several computer programs that implement this approach (e.g., Ref. [2]), and impressive agreement between theoretical calculations and experimental data has been achieved for nuclei with $A \leq 40$ [3,4].

The shell-model approach is limited primarily by the combinatorial growth in the number of basis states with both the number of valence particles (N_v) and the size of the single-particle basis (N_s). Indeed, for nuclei with $A \sim 60$, an unrestricted shell-model calculation utilizing the $0f_{7/2}$-$0f_{5/2}$-$1p_{3/2}$-$1p_{1/2}$ orbits would involve approximately 2×10^9 basis states with definite z projection of angular momentum [5]. Angular momentum and isospin projection would reduce the size of the basis to about 10^7. Clearly, a problem of this magnitude lies beyond the capability of today's computers.

The traditional approach to circumvent the computational limitations inherent in the shell model is to impose what are often severe and *ad hoc* truncations on the number of basis states. Unfortunately, because of the strong character of the residual interaction, calculations of this nature can be unreliable, and significant renormalizations of the residual interaction and transition operators are required.

In two previous papers [6,7], we presented a Monte Carlo method that can give an exact treatment of a nuclear shell-model Hamiltonian, H, even in situations where the matrix-diagonalization technique is impractical. It is based on using the imaginary-time propagator $\hat{U} = \exp(-\beta \hat{H})$ to either perform a thermodynamical trace (canonical or grand canonical) at a temperature $T = \beta^{-1}$ or, for large β, to filter a many-body trial state to the exact ground state. By applying the Hubbard-Stratonovich transformation [8], the two-body terms in U are linearized with the introduction of an auxiliary field, and the problem is reduced to a multidimensional integral whose dimensions scale more gently with either N_v or N_s [6,7].

In Ref. [6], the Monte Carlo method was demonstrated with selected results for $N = Z$ even-even nuclei in the $1s$-$0d$ and $0f$-$1p$ shells, while much of the formalism for Monte Carlo approaches to the nuclear shell model is given in detail in Ref. [7]. The purpose of this work is to further demonstrate the feasibility of the technique by presenting systematic results for $N \neq Z$ even-even nuclei, as well as $N = Z$ odd-odd nuclei in the $1s$-$0d$ shell-model space. In addition, we present a Fourier method for evaluating the canonical trace that avoids some of the numerical problems of the activity expansion method presented in Ref. [7]. We also present a method for deducing the nuclear shape from our calculations.

We begin with a very brief description of the formalism for Monte Carlo techniques in Sec. II; Sec. II A describes the new Fourier method for computing the canonical trace. In Sec. III, results obtained for even Ne isotopes (including cranking) and ^{22}Na are given, and in Sec. IV, a method for deducing the nuclear shape is described and applied to these calculations.

II. FORMALISM

In this section, we briefly describe the Monte Carlo approach to the nuclear shell model utilizing auxiliary fields, referring the reader to Ref. [7] for more details.

*Current address: Los Alamos National Laboratory, T-5, Mail Stop B283, P. O. Box 1663, Los Alamos, NM 87545.

In this work, we will consider only the thermal formalism, and so consider the partition function

$$Z = \hat{\mathrm{Tr}} \exp(-\beta \hat{H}), \tag{1}$$

where $\hat{H}$ is a generalized Hamiltonian for the system (which may include Lagrange multipliers constraining particle number or the z projection of the angular momentum), β may be interpreted as an inverse temperature ($T = 1/\beta$), and $\hat{\mathrm{Tr}}$ represents either a grand-canonical trace over all many-body states in the space (denoted by $\hat{\mathrm{Tr}}_G$) or a canonical trace with fixed particle number N_v (denoted by $\hat{\mathrm{Tr}}_{N_v}$). Given the partition function in Eq. (1), the thermal observable of an operator $\hat{O}$ is

$$\langle \hat{O} \rangle = \frac{1}{Z} \hat{\mathrm{Tr}} \left[\hat{O} \exp(-\beta \hat{H}) \right]. \tag{2}$$

We restrict ourselves to Hamiltonians that contain at most two-body terms such that

$$\hat{H} = \sum_{\alpha} \epsilon_{\alpha} a_{\alpha}^{\dagger} a_{\alpha} + \frac{1}{2} \sum_{\alpha\beta\gamma\delta} V_{\alpha\beta\gamma\delta} a_{\alpha}^{\dagger} a_{\beta}^{\dagger} a_{\delta} a_{\gamma} , \tag{3}$$

where $a_{\alpha}^{\dagger}$ and a_{α} are the anticommuting creation and annihilation operators associated with the single-particle state α defined by the complete set of quantum numbers $nljmt_z$ (n, l, j, m, and t_z denote the principal, orbital angular momentum, total single-particle angular momentum, z projection of j, and the third component of the isospin quantum numbers, respectively), and ϵ_{α} and $V_{\alpha\beta\gamma\delta}$ are the single-particle energies and two-body matrix elements of the residual interaction. Given any two-body Hamiltonian of the form Eq. (3), it is possible to find a convenient set of one-body operators $\hat{\mathcal{O}}_{\alpha}$ so that $\hat{H}$ may be written as

$$\hat{H} = \sum_{\alpha} \epsilon_{\alpha} \hat{\mathcal{O}}_{\alpha} + \frac{1}{2} \sum_{\alpha} V_{\alpha} \hat{\mathcal{O}}_{\alpha}^2 . \tag{4}$$

To simplify the imaginary-time propagator $\hat{U}$, the Hubbard-Stratonovich transformation makes use of the identity

$$e^{\frac{1}{2}\Lambda \hat{\mathcal{O}}^2} = \sqrt{\frac{|\Lambda|}{\pi}} \int d\sigma e^{-\frac{1}{2}|\Lambda|\sigma^2 + s\Lambda\sigma\hat{\mathcal{O}}} , \tag{5}$$

where $s = \pm 1$ if $\Lambda \geq 0$ or $\pm i$ if $\Lambda < 0$. In general, the $\hat{\mathcal{O}}_{\alpha}$ do not commute, and when Eq. (5) is applied to $\hat{U}$, the resulting integral is accurate only to order $\beta V_{\alpha} \hat{\mathcal{O}}_{\alpha}^2$. The accuracy is improved by dividing $\hat{U}$ into N_t "time slices," so that $\hat{U} = \left(\exp[-\Delta\beta \hat{H}] \right)^{N_t}$, and applying Eq. (5) to each "slice." For what follows, we introduce τ_n as an imaginary time in the range $(0, \beta)$ defined as $\tau_n = n\Delta\beta$, with $\Delta\beta = \beta/N_t$.

The thermal observable in Eq. (2) can now be written as

$$\langle \hat{O} \rangle = \frac{\int \mathcal{D}[\sigma] \mathcal{G}(\sigma) \langle \hat{O} \rangle_{\sigma} \zeta(\sigma)}{\int \mathcal{D}[\sigma] \mathcal{G}(\sigma) \zeta(\sigma)}, \tag{6}$$

where $\mathcal{D}[\sigma] = \prod_{n,\alpha} d\sigma_{\alpha}(\tau_n)$ is the volume element,

$$\mathcal{G}(\sigma) = \exp[-\frac{1}{2}\Delta\beta \sum_{\alpha,n} |V_{\alpha}| \sigma_{\alpha}^2(\tau_n)],$$
$$\zeta(\sigma) = \hat{\mathrm{Tr}}[\hat{U}_{\sigma}(\beta, 0)] \tag{7}$$

is a trace over the one-body imaginary-time evolution operator, and

$$\langle \hat{O} \rangle_{\sigma} = \frac{\hat{\mathrm{Tr}} \left[\hat{O} \hat{U}_{\sigma}(\beta, 0) \right]}{\hat{\mathrm{Tr}} \left[\hat{U}_{\sigma}(\beta, 0) \right]}. \tag{8}$$

In these expressions, the one-body evolution operator is defined as

$$\hat{U}_{\sigma}(\tau_j, \tau_i) = \hat{U}(\sigma(\tau_j)) \ldots \hat{U}(\sigma(\tau_{i+1})) \hat{U}(\sigma(\tau_i)) , \tag{9}$$

with

$$\hat{U}(\sigma) = \exp \left[-\Delta\beta \hat{h}(\sigma) \right], \tag{10}$$

and

$$\hat{h}(\sigma) = \sum_{\alpha} (\epsilon_{\alpha} + s_{\alpha} V_{\alpha} \sigma_{\alpha}) \mathcal{O}_{\alpha}. \tag{11}$$

In this work, we have chosen the density-decomposition described in Ref. [7], where the $\hat{\mathcal{O}}_{\alpha}$ are linear combinations of the proton and neutron multipole-density operators $\rho^{KM}(a, b) = [a_a^{\dagger} \times \tilde{a}_b]^{KM}$. Written in this way, $h(\sigma)$ can be constructed from operators that act on protons or neutrons separately, leading to separate proton and neutron traces; i.e., $\zeta_A(\sigma) = \zeta_Z(\sigma)\zeta_N(\sigma)$. Of course, N_v and N_s then generically represent the number of valence protons or neutrons and single-particle states.

Equation (6) expresses the expectation value of any observable as a multidimensional integral whose dimensions are at most $N_s^2 \cdot N_t$, so that it must be evaluated by Monte Carlo techniques. Towards this end, it is necessary to define a positive-definite weight function $W(\sigma)$. In this work, we chose $W(\sigma) = \mathcal{G}(\sigma)|\zeta(\sigma)|$ so that

$$\langle \hat{O} \rangle = \frac{\int \mathcal{D}[\sigma] W(\sigma) \langle \hat{O} \rangle_{\sigma} \Phi(\sigma)}{\int \mathcal{D}[\sigma] W(\sigma) \Phi(\sigma)}, \tag{12}$$

with the "sign" $\Phi(\sigma) \equiv \zeta(\sigma)/|\zeta(\sigma)|$. The observable $\langle \hat{O} \rangle$ is then computed by selecting an ensemble $\{\sigma_k\}$ chosen according to distribution $W(\sigma)$, and computing the ensemble average; i.e.,

$$\langle \hat{O} \rangle = \frac{\sum_k \langle \hat{O} \rangle_{\sigma_k} \Phi(\sigma_k)}{\sum_k \Phi(\sigma_k)}. \tag{13}$$

The uncertainty in the Monte Carlo result is then related to the ensemble standard deviation (taking into account possible correlations between the numerator and denominator [7]). We have chosen the σ_n using the standard algorithm of Metropolis *et al.* [9]. Note that a potential problem in the Monte Carlo method is that the sign

should be well determined. If $\Phi(\sigma_k)$ oscillates wildly from sample to sample, then large errors occur in $\langle\hat{O}\rangle$ because of the poorly determined numerator and denominator in Eq. (13).

Some remarks about the nature of the operators in Eq. (6) and their notation are now in order. First, since $\hat{h}(\sigma)$ is only a one-body operator, the evolution operator $\hat{U}(\sigma)$ can be represented as a $N_s \times N_s$ matrix $\boldsymbol{U}(\sigma)$ in the single-particle basis: $\boldsymbol{U}(\sigma) = \exp[-\Delta\beta\boldsymbol{h}(\sigma)]$, where $[\boldsymbol{h}(\sigma)]_{\alpha\beta} = \langle\alpha|\hat{h}(\sigma)|\beta\rangle$. Likewise, any Slater determinant $|\psi_S\rangle$ describing N_v particles can be represented by a matrix with N_v columns and N_s rows. Thouless' theorem then implies that the operation $\hat{U}(\sigma)|\psi_S\rangle$ yields only a single Slater determinant, thus averting the need to have all Slater determinants stored in order to evaluate Eq. (2). In what follows, we represent the product of one-body evolution operators $\hat{U}_\sigma(\tau_j,\tau_i)$ as

$$\boldsymbol{U}_\sigma(\tau_j,\tau_i) = \boldsymbol{U}(\sigma(\tau_j))\cdots\boldsymbol{U}(\sigma(\tau_{i+1}))\boldsymbol{U}(\sigma(\tau_i)) , \quad (14)$$

with the implicit understanding that $\boldsymbol{U}_\sigma(\beta,0) = \boldsymbol{U}_\sigma$.

Given the matrix notation for $\hat{U}_\sigma(\beta,0)$, the grand-canonical trace is given by

$$\hat{\mathrm{Tr}}_G[\hat{U}_\sigma(\beta,0)] = \det(\mathbf{1}+\boldsymbol{U}_\sigma) . \quad (15)$$

The canonical trace for fixed particle number N_v, $\zeta_{N_v}(\sigma)$, can be obtained from an activity expansion by noting that [7]

$$\begin{aligned}\det(\mathbf{1}+\lambda\boldsymbol{U}_\sigma) &= \sum_{N=0}^{N_s}\lambda^N\zeta_N(\sigma)\\ &= \exp\{\mathrm{tr}[\ln(\mathbf{1}+\lambda\boldsymbol{U}_\sigma)]\}\\ &= \exp\left(\sum_{n=1}^{N_s}\frac{(-1)^{n-1}}{n}\lambda^n\mathrm{tr}[\boldsymbol{U}_\sigma^n]\right), \end{aligned} \quad (16)$$

where the symbol "tr" denotes a matrix trace.

A. Fourier method for the canonical trace

A major drawback of the activity expansion for computing the canonical trace is that for $N_v \approx N_s/2$ (i.e., near half filling), $\zeta_{N_v}(\sigma)$ involves a sum of terms that are large in magnitude and have alternating signs. In practical terms, the activity expansion is unstable in the midshell region because these terms cancel in the sum to 10–14 orders of magnitude, and there is a loss of numerical precision in the evaluation of Eq. (7). In actual calculations, we have found the activity expansion to be stable only for $N_v \leq 4$, or, using an equivalent hole formalism, for $N_v \geq N_s - 4$.

An alternative procedure for computing the canonical trace is to use Fourier extraction. Starting from the grand-canonical trace, and defining $\phi_m = 2\pi m/N_s$, we may write

$$\det\left[\mathbf{1}+e^{i\phi_m}e^{\beta\mu}\boldsymbol{U}_\sigma\right] = \sum_{N=0}^{N_s}e^{i\phi_m N}e^{\beta\mu N}\zeta_N(\sigma) , \quad (17)$$

where μ is a parameter introduced to insure numerical stability throughout the range of particles in the model space, and is given below. Using the identity

$$\frac{1}{N_s}\sum_{m=1}^{N_s}e^{i\phi_m K} = \delta_{K0}, \quad (18)$$

valid for integer K, we find

$$\begin{aligned}\zeta_{N_v}(\sigma) = \frac{1}{N_s}\sum_{m=1}^{N_s}&e^{-i\phi_m N_v}e^{-\beta\mu N_v}\\ &\times\det\left[\mathbf{1}+e^{i\phi_m}e^{\beta\mu}\boldsymbol{U}_\sigma\right].\end{aligned} \quad (19)$$

The expectation values of the one- and two-body density operators can be computed in a similar fashion:

$$\begin{aligned}\langle a_\alpha^\dagger a_\beta\rangle_{\sigma,N_v} = \frac{1}{N_s\zeta_{N_v}(\sigma)}&\sum_{m=1}^{N_s}e^{-iN_v\phi_m}e^{-\beta N_v\mu}\\ &\times\eta_m(\sigma)\gamma_{\alpha\beta}^m(\sigma),\end{aligned} \quad (20)$$

and

$$\begin{aligned}\langle a_\alpha^\dagger a_\beta a_\gamma^\dagger a_\delta\rangle_{\sigma,N_v} = \frac{1}{N_s\zeta_{N_v}(\sigma)}&\sum_{m=1}^{N_s}e^{-iN_v\phi_m}e^{-\beta N_v\mu}\eta_m(\sigma)\\ &\times\Big[\gamma_{\alpha\beta}^m(\sigma)\gamma_{\gamma\delta}^m(\sigma)-\gamma_{\alpha\delta}^m(\sigma)\gamma_{\gamma\beta}^m(\sigma)\\ &+\delta_{\beta\gamma}\gamma_{\alpha\delta}^m(\sigma)\Big],\end{aligned} \quad (21)$$

where

$$\eta_m(\sigma) = \det\left[\mathbf{1}+e^{i\phi_m}e^{\beta\mu}\boldsymbol{U}_\sigma\right] \quad (22)$$

and

$$\gamma_{\alpha\beta}^m(\sigma) = \left[(\mathbf{1}+e^{i\phi_m}e^{\beta\mu}\boldsymbol{U}_\sigma)^{-1}e^{i\phi_m}e^{\beta\mu}\boldsymbol{U}_\sigma\right]_{\beta\alpha} . \quad (23)$$

The observables in Eqs. (19)–(21) are, of course, independent of the value of μ chosen. However, as the ζ_n vary rapidly with N, a good choice for μ is one for which the sum in Eq. (17) peaks at $N = N_v$. In order to find a good choice for μ, we first find the N_s eigenvalues, λ_i of U_σ, where $i = 1,...,N_s$, and $|\lambda_1| < |\lambda_2| < \cdots$ (note that each eigenvalue has the form $|\lambda_i| = \exp[-\beta\varepsilon_i]$). Thus, for the valence particles, we define μ by

$$\begin{aligned}|\lambda_{N_v}\lambda_{N_v+1}|^{1/2} &= \exp\left[-\beta\frac{\mathrm{Re}\varepsilon_{N_v}+\mathrm{Re}\varepsilon_{N_v+1}}{2}\right]\\ &= \exp[-\beta\mu] .\end{aligned} \quad (24)$$

This prescription allows us to use Fourier extraction for all even-even nuclei in both the *sd* and *fp* shells.

At first glance, the Fourier method appears to add substantial computational effort since the computation of a determinant scales as N_s^3 and it must be computed N_s times in Eq. (19). In fact, the computation of ζ_{N_v} can be simplified considerably by computing the N_s eigenvalues, λ_i, of $\boldsymbol{U}_\sigma$, in terms of which, the factor $\eta_m(\sigma)$ can be written as

$$\eta_m(\sigma) = \prod_{i=1}^{N_s}(1 + e^{i\phi_m}e^{\beta\mu}\lambda_i). \quad (25)$$

In addition, the matrix $\gamma^m_{\alpha\beta}(\sigma)$ is given by

$$\gamma^m_{\alpha\beta}(\sigma) = \sum_\delta P_{\beta\delta}(1 + e^{i\phi_m}e^{\beta\mu}\lambda_\delta)^{-1}e^{i\phi_m}P^{-1}_{\delta\alpha}\,, \quad (26)$$

where $\boldsymbol{P}$ is the transformation matrix associated with the diagonalization of $\boldsymbol{U}_\sigma$.

III. RESULTS

In Refs. [6,7], results obtained with the Monte Carlo approach to the nuclear shell model were presented for even-even $N = Z$ nuclei using a pairing plus multipole-multipole interaction. We found empirically, and later proved for the zero-temperature and grand-canonical formalisms [7], that under certain conditions the sign $\Phi(\sigma)$ in the Monte Carlo sampling is always unity. These conditions are that in the density decomposition, the sign of V_α is given by $(-1)^K$, where K is the angular momentum rank of the operator $\hat{O}_\alpha$, and either (i) $N = Z$ or (ii) the number of protons and neutrons is even. When a Lagrange multiplier ω is used to constrain the z component of the angular momentum, $\hat{J}_z$, (i.e., cranking with $\hat{H}' = \hat{H} - \omega\hat{J}_z$), the time-reversal symmetry used to prove these statements is broken, and the sign need not be unity.

In this section, we further demonstrate the viability of the Monte Carlo shell-model approach by presenting calculations for $N \neq Z$ even-even and $N = Z$ odd-odd nuclei using the $1s$-$0d$ shell-model configuration space. The interaction was chosen to be of the pairing plus multipole form similar to that used in Refs. [6,7] (the exact parameters can be obtained from the authors). In each of the calculations presented, we used $\Delta\beta = 0.0625$ and approximately 2000 Monte Carlo samples were collected. The independence of the individual samples was tested by computing the autocorrelation function for $\langle H\rangle_\sigma$. All the calculations presented here were performed on the Intel Touchstone Gamma and Delta systems operated by Caltech for the Concurrent Supercomputer Consortium.

We begin with a compendium of results for the Ne isotopes. We show in Fig. 1 the expectation values (open symbols) (a) $\langle\hat{H}\rangle$, (b) $\langle Q^2\rangle$ (quadrupole moment), (c) $\langle J^2\rangle$ (angular momentum), and (d) $\langle T^2\rangle$ (isospin) as functions of β for even-even Ne isotopes. Exact calculations within the canonical ensemble for ^{20,22}Ne using the eigenvalues obtained from the shell-model code OXBASH [2] are indicated by the curves in the figure. In addition, the ground-state observables are plotted using solid symbols at $\beta = 2.5$. Generally, we see that the Monte Carlo procedure is in good agreement with the exact calculations. Shown in Fig. 2 are the results for the same quantities for the odd-odd $N = Z$ nucleus ^{22}Na.

In Ref. [7], we described how the strength function, $f(E)$, for the operator $\hat{O}$ can be computed using the maximum entropy (MaxEnt) technique to perform the inverse Laplace transform on the imaginary-time correlation function $\langle\hat{O}(\tau)\hat{O}(0)\rangle = \hat{\mathrm{T}}\mathrm{r}[e^{-\beta H}e^{\tau H}\hat{O}e^{-\tau H}\hat{O}]$. For demonstration purposes, we display the results for ^{22}Ne at $\beta = 2.0$ (16 and 32 time slices) in Fig. 3 for (a) the isoscalar quadrupole, $\langle Q^0(\tau)\cdot Q^0(0)\rangle$, (b) the isovector quadrupole, $\langle Q^1(\tau)\cdot Q^1(0)\rangle$, and (c) the isovector angular momentum, $\langle J^1(\tau)\cdot J^1(0)\rangle$, in Fig. 4. Generally, the reconstructed strength functions are in good agreement with the exact results, especially in those cases where most of the strength is concentrated in a single peak as for the isoscalar quadrupole. For the situation in which the strength function is strongly fragmented, as in the case for the isovector angular momentum, the various lines can be reconstructed only by using many more time slices so that sufficient information in the small τ region of the imaginary-time response function exits. It is clear that in this case it is necessary to disentangle several decaying exponentials with different slopes.

We may also study rotating nuclei using the crank-

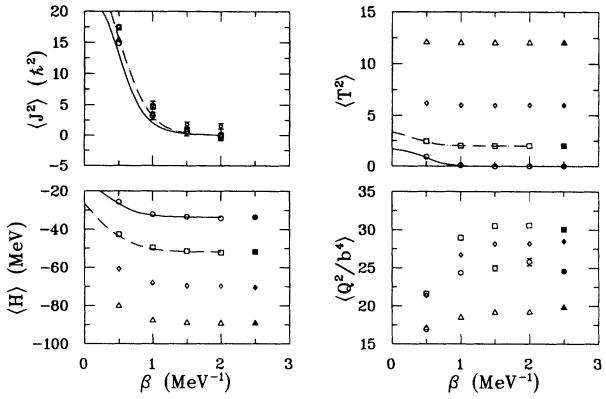

FIG. 1. The results of the Monte Carlo calculation for the expectation values of (a) $\langle\hat{H}\rangle$, (b) $\langle Q^2\rangle$, (c) $\langle J^2\rangle$, and (d) $\langle T^2\rangle$ as a function of β for ^{20}Ne (circles), ^{22}Ne (squares), ^{24}Ne (diamonds), and ^{26}Ne (triangles). Where absent, the error bars are smaller than the size of the symbols. The solid (^{20}Ne) and dash-dotted (^{22}Ne) lines indicate the canonical results obtained from the eigenvalues of an exact diagonalization. The ground-state expectation value for each nucleus is plotted with a solid symbol at $\beta = 2.5$ (except for J^2, for which the ground-state value is zero for all nuclei).

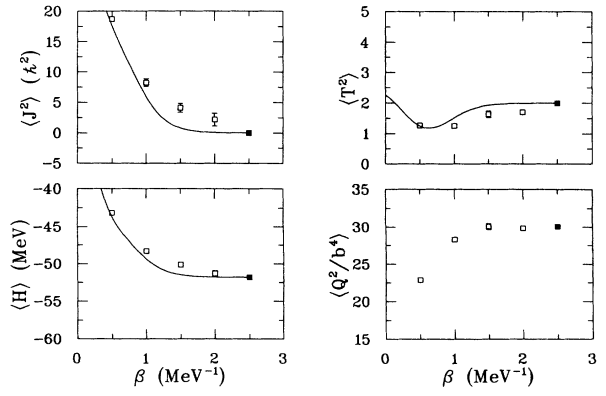

FIG. 2. Same as Fig. 1 for ^{22}Na.

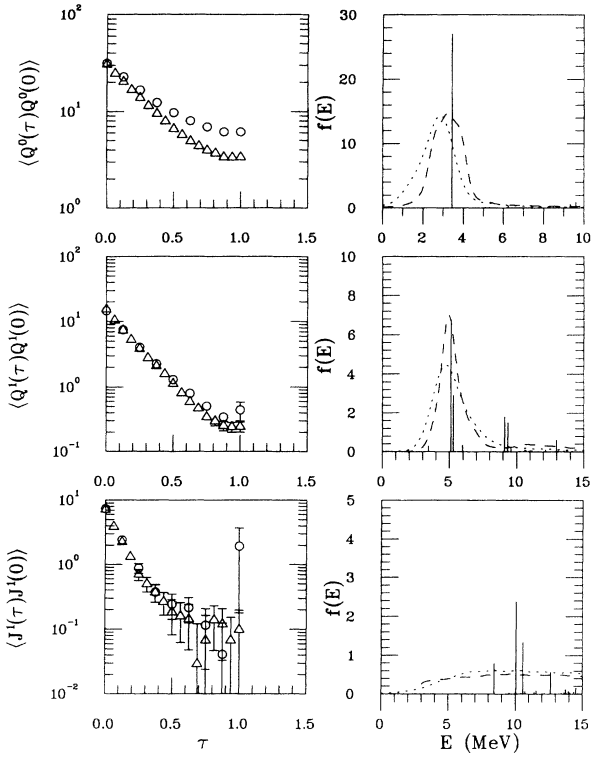

FIG. 3. Response functions for ^{22}Ne are shown, along with MaxEnt (maximum entropy) reconstruction of the strength functions. The calculated response functions (left) of the isoscalar quadrupole (top), isovector quadrupole (middle), and isovector angular momentum (bottom) are shown for $\Delta\beta = 0.125$ (circles), and $\Delta\beta = 0.0625$ (triangles). MaxEnt reconstruction of the strength functions are also given for $\Delta\beta = 0.125$ (dotted line) and $\Delta\beta = 0.0625$ (dashed line). Exact results given as the delta function peaks.

ing Hamiltonian, $\hat{H}' = \hat{H} - \omega J_z$. This procedure has also been discussed in Ref. [7], and we indicate here how cranking affects an $N \neq Z$ nuclei such as ^{22}Ne. The systematics for cranking ^{22}Ne are shown in Fig. 4, where we display $\langle \hat{H} \rangle$, $\langle \hat{J}_z \rangle$, and the sign $\langle \Phi \rangle$ as a function of β and ω. We find that the sign decays rapidly as both the cranking frequency and β increase. The maximum J_z available to ^{22}Ne is 10, and, therefore, the $\omega = 2$ case can be considered as an extreme limit.

A. Nuclear shapes

It is of particular interest to determine the quadrupole shape of a nucleus as function of temperature and angular momentum. It is generally expected that some nuclei may exhibit a sudden phase transition from a prolate to spherical shape as the temperature increases [10]. In addition, as the cranking frequency is increased a transition to oblate ellipsoids is also expected.

One measure of the quadrupole deformation is the expectation value of Q^2. As is illustrated in the proceeding section, $\langle Q^2 \rangle$ is considerably larger for nuclei that are expected to exhibit prolate deformations such as ^{20,22,24}Ne, and is much smaller for spherical nuclei such as ^{26}Ne;

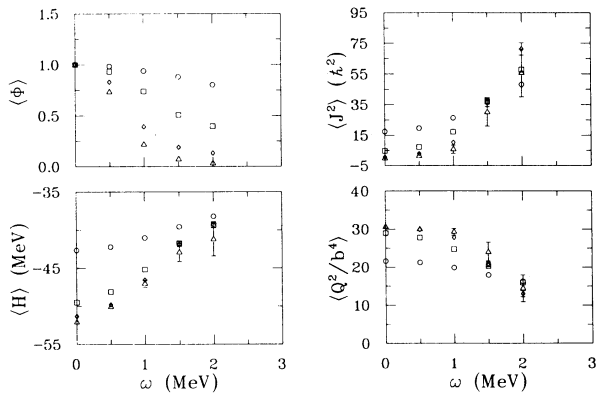

FIG. 4. Cranked results for ^{22}Ne are given as a function of the cranking frequency ω. Calculations were performed at $\beta = 0.5$ (circles), 1.0 (squares), 1.5 (diamonds), and 2.0 (triangles).

however, $\langle Q^2 \rangle$ suffers from two shortcomings. First, Q^2 contains a one-body term proportional to $\langle r^4 \rangle$, which is present even for spherical nuclei, and tends to obscure the contribution due to the nuclear deformation. In addition, $\langle Q^2 \rangle$ does not distinguish between prolate and oblate shapes.

In order to obtain a more detailed picture of the deformation, we examine the components of the quadrupole operator $Q_\mu = r^2 Y^*_{2\mu}$. Note, however, that due to rotational invariance of the Hamiltonian, the expectation value of any component Q_μ is expected to vanish. On the other hand, for each Monte Carlo sample, there exists an intrinsic frame in which it is possible to compute the three nonzero components Q'_0, Q'_2, and Q'_{-2} (the prime is used to denote the intrinsic frame). The intrinsic quadrupole moments can then be related to the standard deformation coordinates β and γ [11] by

$$\begin{aligned}
\langle Q'_0 \rangle_\sigma &= \frac{3}{2\pi}\sqrt{\frac{4\pi}{5}}\langle r^2 \rangle_\sigma \beta_\sigma \cos\gamma_\sigma \ , \\
\langle Q'_2 \rangle_\sigma &= \frac{3}{2\pi}\sqrt{\frac{4\pi}{5}}\langle r^2 \rangle_\sigma \frac{\beta_\sigma}{\sqrt{2}} \sin\gamma_\sigma \ , \\
\langle Q'_{-2} \rangle_\sigma &= \frac{3}{2\pi}\sqrt{\frac{4\pi}{5}}\langle r^2 \rangle_\sigma \frac{\beta_\sigma}{\sqrt{2}} \sin\gamma_\sigma \ .
\end{aligned} \tag{27}$$

The task remains to compute the quadrupole moments in the intrinsic frame for each Monte Carlo sample. This is accomplished by computing and diagonalizing the expectation value of the Cartesian quadrupole tensor $Q_{ij} = 3x_i x_j - \delta_{ij} r^2$ for each Monte Carlo sample. From the three eigenvalues, it is straightforward to determine the deformation parameters as [12]

$$\begin{aligned}
\langle Q'_{11} \rangle_\sigma &= \sqrt{\frac{2\pi}{5}}\left[\sqrt{3}(\langle Q'_2 \rangle_\sigma + \langle Q'_{-2} \rangle_\sigma) - \sqrt{2}\langle Q'_0 \rangle_\sigma\right] \ , \\
\langle Q'_{22} \rangle_\sigma &= \sqrt{\frac{2\pi}{5}}\left[-\sqrt{3}(\langle Q'_2 \rangle_\sigma + \langle Q'_{-2} \rangle_\sigma) - \sqrt{2}\langle Q'_0 \rangle_\sigma\right] \ , \\
\langle Q'_{33} \rangle_\sigma &= 2\sqrt{\frac{4\pi}{5}}\langle Q'_0 \rangle_\sigma .
\end{aligned} \tag{28}$$

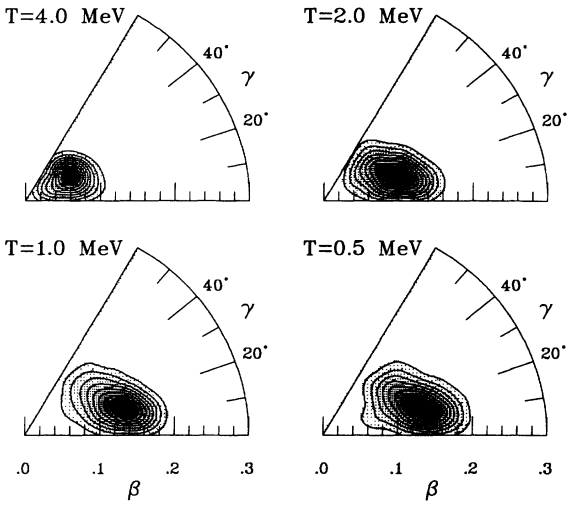

FIG. 5. Distribution functions $F(\beta,\gamma)$ are shown for ^{22}Ne at different temperatures T.

Note that from Eq. (27) one finds $Q'_{22} \leq Q'_{11} \leq Q'_{33}$.

To illustrate the intrinsic deformation, we plot in Fig. 5 the distribution function $F(\beta,\gamma) = f(\beta,\gamma)\beta^4 \sin(3\gamma)$ for temperatures $T = 0.5$, 1.0, 2.0, and 4.0 MeV. The distribution function was computed from the set of the β and γ values from each Monte Carlo sampled, and then smoothed with a symmetric Gaussian with a width of 0.01. Although the volume element $\beta^4 \sin(3\gamma)$ tends to push the function towards $\gamma = \pi/6$, there is a definite trend from a prolate deformation at low temperature to a symmetric spherical shape at higher temperatures.

IV. CONCLUSIONS

We have further demonstrated the utility of using path integral methods in the nuclear shell model. We have used a realistic pairing plus multipole interaction for *sd*-shell nuclei, and have demonstrated systematics in the neon system. In order to evaluate midshell quantities in the canonical formalism, we introduced the Fourier extraction method. We have also indicated how shape changes in nuclei may be calculated and observed.

In future work (in progress) we will study shape changes and behavior of the rare-earth nuclei using the pairing plus multipole interactions. These calculations, the largest to date, have nearly 100 000 fields over which to integrate. We also wish to further investigate the 'minus sign' problem inherent in these calculations when certain interaction schemes are used.

This work was supported in part by the National Science Foundation (Grants No. PHY90-13248 and PHY91-15574). W.E.O. would like to thank the Weingart Foundation for financial support.

[1] P. J. Brussaard and P. W. M. Glaudemans, *Shell-Model Applications in Nuclear Spectroscopy* (North Holland, Amsterdam, 1977); R. D. Lawson, *Theory of the Nuclear Shell Model* (Clarendon, Oxford, 1980).

[2] W. D. M. Rae, A. Etchegoyen, and B. A. Brown, "OXBASH, The Oxford-Buenos Aires-MSU shell-model code," Michigan State University Cyclotron Laboratory Report No. 524, 1988.

[3] B. H. Wildenthal, in *Progress in Particle and Nuclear Physics*, edited by D. H. Wilkinson (Pergamon, Oxford, 1984), Vol. 11, p. 5.

[4] B. A. Brown and B. H. Wildenthal, Ann. Rev. Nucl. Part. Sci. **38**, 29 (1988).

[5] T. Sebe and M. Harvey, "Enumeration of many body states of the nuclear shell model with definite angular momentum and isobaric spin with mixed single particle orbits," Atomic Energy of Canada Limited, Report No. AECL-3007, 1968.

[6] C. W. Johnson, S. E. Koonin, G. H. Lang, and W. E. Ormand, Phys. Rev. Lett. **69**, 3157 (1992).

[7] G. H. Lang, C. W. Johnson, S. E. Koonin, and W. E. Ormand, Phys. Rev. C **48**, 1518 (1993).

[8] J. Hubbard, Phys. Rev. Lett. **3**, 77 (1959); R. L. Stratonovich, Dokl. Akad. Nauk. SSSR **115**, 1097 (1957) [Sov. Phys. Dokl. **2**, 416 (1958)].

[9] N. Metropolis, A. Rosenbluth, M. Rosenbluth, A. Teller, and E. Teller, J. Chem. Phys. **21**, 1087 (1953).

[10] S. Levit and Y. Alhassid, Nucl. Phys. **A413**, 439 (1984).

[11] A. Bohr and B. R. Mottelson, *Nuclear Structure* (Benjamin, Reading, MA, 1975), Vol. II.

[12] J. D. Jackson, *Classical Electrodynamic* (Wiley, New York, 1962).

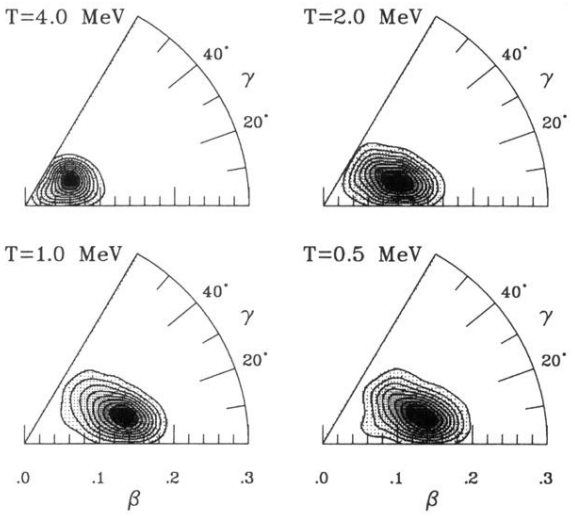

FIG. 5. Distribution functions $F(\beta, \gamma)$ are shown for ^{22}Ne at different temperatures T.